Developing on-machine 3D profile measurement for deterministic fabrication of aspheric mirrors

Zhichao Dong,[1] Haobo Cheng,[1,*] Xu Ye,[1] and Hon-Yuen Tam[2]

[1]School of Optoelectronics, Beijing Institute of Technology University, Haidian District, Beijing 100081, China

[2]Department of Mechanical and Biomedical Engineering, City University of Hong Kong, Hong Kong 999077, China

*Corresponding author: chenghaobo@tsinghua.org.cn

Received 12 May 2014; revised 26 June 2014; accepted 27 June 2014;
posted 30 June 2014 (Doc. ID 211911); published 25 July 2014

Three-dimensional profile measurement is perceived as an indispensable process for deterministic fabrication of aspheric mirrors. In this work, we develop on-machine 3D profile measurement on a subaperture polishing machine, namely, JR-1800. The influences of mechanical errors, misalignments, output stability, temperature variation, and natural vibration are investigated in detail by calibration, mechanical alignment, and finite-element analysis. Two quantitative methods are presented for aligning the turntable, length gauge, and workpiece into together. An error compensation model is also developed for further eliminating misalignments. For feasibility validation, two prototypical workpieces are measured by JR-1800 and an interferometer. The results indicate that JR-1800 has an RMS repeatability of $\sim\lambda/30$ ($\lambda = 632.8$ nm). The data provided by the two systems are highly coincident. Direct subtractions of the results from the two systems indicate that the RMS deviations for both segments are less than 0.07 μm.

OCIS codes: (220.4610) Optical fabrication; (120.0120) Instrumentation, measurement, and metrology; (120.6650) Surface measurements, figure.

http://dx.doi.org/10.1364/AO.53.004997

1. Introduction

Aspheric segments, such as paraboloids and hyperboloids, are widely used in modern and next-generation optical systems, such as intense laser systems, telescopes for astro-observation, photolithography systems, etc. Compared with spheres, aspherics have advantages of improving image quality, and reducing size and weight, which are significant for space instruments (e.g., space cameras and telescopes). However, due to inconsistency of curvature, the fabrication and metrology of aspheric mirrors are prone to be more difficult.

Currently, the fabrication of aspheric mirrors involves three stages: (1) grinding work-blanks into desired shapes with various diamond tools [1]; (2) iterative lapping to diminish surface roughness, control geometrical constants, and remove most subsurface damages [2,3]; and (3) iterative deterministic polishing for further improving the surface form and roughness. The last two stages can improve the surface peak to valley (PV) from tens of micrometers to tens of nanometers [4,5], which relies on the surface form measured by interferometers or other profilers to close the feedback manufacturing loop. Generally speaking, due to insufficient versatility, these grinding, lapping, polishing, and measuring instruments require cooperation to finish a task.

With respect to specular aspheric mirrors, various interferometric methods have been developed, such as null lens compensators [6], subaperture stitching [7], computer-generated holograms [8], etc. However, ground blanks in the lapping stage with a rough (i.e., nonspecular) surface could not meet the interferometric requirement of a He–Ne laser. To measure these blanks, one candidate is an infrared interferometer [9]. However, it is (1) expensive due to its

1559-128X/14/224997-11$15.00/0

expensive infrared devices; (2) has low sensitivity because of the longer laser wavelength (e.g., 10.6 μm for CO_2 laser); and (3) is still dependent on null compensators for measuring aspherics. A commercialized coordinate measurement machine (CMM) is also an alternative. Form Talysurf PGI 1240 (Taylor Hobson) is commonly used for measuring the surface profile, but its gauge range (~12.5 mm) and traverse range (~200 mm) are not enough for large aspherics (e.g., meter scale). The multiprobe bar profilometer developed by Itek [10] utilizes a high-precision sphere and multi-LVDT (linear variable differential transformer) sensors for comparison measurement, which has an accuracy of 0.15 μm RMS. However, it needs a high-precision reference sphere, which is costly and complex. Comley *et al.* [1] and Gray *et al.* [11] reported the profile data of E-ELT segments (1.4 m size) measured with an off-machine Leitz CMM. Su and co-workers investigated a swing arm profilometer for *in situ* measurement of aspherics. The machine adopts a sphere coordinate and can be calibrated by a dual probe, which achieves submicron accuracy [12,13]. Jing and co-workers [14,15] also reported a swing arm profilometer; they employed a model to raise accuracy to 0.2 μm. Researchers also developed on-machine measurements for increasing fabrication accuracy [16]. Compared with off-machine measurement, on-machine measurement does not need remounting and realigning workpieces, which is time-saving and less risky.

This work presents a multifunctional system, namely, JR-1800 [17] that is competent for these fabrication and metrology works. It possesses bound and loose abrasive lapping, polishing, and on-machine 3D profile measurement for plane, sphere, and aspheric mirrors. Compared with single-purpose machines, it can (1) omit the remounting and realignment works; (2) reduce risks when carrying workpieces from one machine to another; and (3) largely save cost and space. The mechanical errors of JR-1800, misalignments of the length gauge and workpieces, output stability of the length gauge, temperature variation, and natural vibration are investigated by data calibration, precision alignments, and finite-element analysis (FEA), respectively, which can be found in Section 3. This is followed by tool radius compensation and misalignment compensation as detailed in Section 4. The two verification experiments in Section 5 demonstrate the feasibility of JR-1800 for use for 3D profile measurement of aspheric mirrors in lapping and initial polishing stages.

2. Background of Profile Measurement

A. Aspheric Surfaces

Aspheric surfaces frequently used in optical systems can be expressed by Eq. (1), where C denotes the curvature of the aspherical surfaces ($C = 1/R$, where R is the vertex radius of curvature), K is the conic constant, n refers to the aspheric order, and A_{2i} indicates the high-order aspheric coefficient:

$$Z(X,Y) = \frac{C(X^2+Y^2)}{1+\sqrt{1-(K+1)C^2(X^2+Y^2)}} + \sum_{i=1}^{n} A_{2i}(X^2+Y^2)^i. \tag{1}$$

In particular, off-axis aspherics are now popular in spaced three reflective cameras, collimating devices, etc., of whom one off-center portion (OA-I) of a symmetric parent mirror is shown in Fig. 1. Its surface equation in $(O_1 - X_1Y_1Z_1)$ can be defined by Eq. (2), where (y_0, z_0) refer to the coordinate of O_1 in the parent mirror. Another off-axis aspheric mirror (OA-II) seems to be symmetric, which is cut from OA-I. The surface definition can be obtained by rotating Eq. (2) along X_1 axis by a rotating angle θ. According to the coordinate transform theory, point (X', Y', Z') should satisfy Eq. (3). Combining Eqs. (2) and (3) yields Eq. (4) and can be simplified as Eq. (5) as the theoretical surface equation of OA-II:

$$Z_1(X,Y) = \frac{C(X_1^2+(Y_1-y_0)^2)}{1+\sqrt{1-(K+1)C^2(X_1^2+(Y_1-y_0)^2)}} - z_0, \tag{2}$$

$$\begin{vmatrix} X' \\ Y' \\ Z' \\ 1 \end{vmatrix} = \begin{vmatrix} 1 & 0 & 0 & 0 \\ 0 & \cos(\theta) & -\sin(\theta) & 0 \\ 0 & \sin(\theta) & \cos(\theta) & 0 \\ 0 & 0 & 0 & 1 \end{vmatrix} \begin{vmatrix} X_1 \\ Y_1 \\ Z_1 \\ 1 \end{vmatrix}, \tag{3}$$

$$AZ'^2 + BZ' + Q = 0, \tag{4}$$

$$Z' = \frac{-B+\sqrt{B^2-4AQ}}{2A}, \tag{5}$$

where

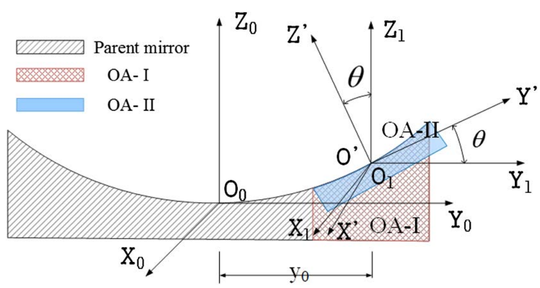

Fig. 1. Sketch map of aspheric surfaces.

$$
\begin{cases}
A = C + KC\cos^2(\theta) \\
B = (-2CY'\sin(\theta)\cos(\theta) - 2Cy_0\ \sin(\theta) - 2\ \cos(\theta) \\
+(K+1)C(2z_0\ \cos(\theta) + 2Y'\sin(\theta)\cos(\theta))) \\
Q = 2z_0 + 2Y'\ \sin(\theta) - (K+1)C(z_0^2 + 2Y'z_0\ \sin(\theta) \\
+Y'^2\sin^2(\theta)) - C(X'^2 + Y'^2\cos^2(\theta) \\
+2Y'y_0\ \cos(\theta) + y_0^2)
\end{cases}. \tag{6}
$$

B. On-Machine Measurement System JR-1800

As shown in Fig. 2(a), JR-1800 is a multifunctional system developed in 2012 for precision fabrication and measurement of large optical mirrors, especially, aspheric mirrors. It adopts a gantry structure on a base marble of 3200 mm × 4000 mm × 620 mm, which is supported by a vibration-free groundwork. It comprises four main parts: XYZ axis (stroke: 1840 mm × 2096 mm × 603 mm), a Φ1800 mm rotating turntable (C axis) supporting workpieces, a changeable metrology unit with a length gauge attached at the end of Z axis, and a swingable fabrication unit (SAB axis). The fabrication unit can track the normal direction of aspherics by the swing axis (S axis). The maximal metrology and fabrication range reaches up to 1800 mm for plane, sphere, and aspherics. Figure 2(b) presents the lateral view of the fabrication and metrology unit with a 153 mm × 298 mm × 148 mm spaced offset. Figure 2(c) shows the fabrication status; the length gauge would retract to keep away from the workpieces. Figure 2(d) presents the metrology status; the fabrication unit is rotated in the horizontal direction. Thus, the fabrication and metrology would be independent and not disturb mutually, and there is no need to remount and realign the length gauge for every measurement.

A commercially available digital length gauge MT60 (Heidenhain) with a touch-trigger probe is mounted as a contact sensor. MT60 employs an optical linear encoder to measure the extended length of its plunger with a maximal stroke of 60.8 mm, which is larger than the maximal sagittal height of most meter-scale spheres and aspherics. Therefore, the Z axis can remain dormant during measurement, which eliminates errors induced by the positioning error of Z axis. On the other hand, as shown in Fig. 2(b), the Abbe offset (225.7 mm, between the Z axis slide and the plunger of MT60) would induce Abbe error if the Z axis is moved. However, this error is avoided by keeping Z axis dormant. The design of JR-1800 meets the Abbe measurement principle that the ruler should coincide with the distance to be measured.

JR-1800 can measure optical segments in XY and XC modes, which scan a segment by the combination of XY axis and XC axis, respectively. It samples a series of discrete data by virtue of MT60 and then yields a surface form by comparing the measured surface with the ideal surface.

Compared with laser interferometers, the characteristics of JR-1800 can be summarized as follows:

(1) JR-1800 is suitable for any kind of surface shape, including plane, sphere, aspheric, and free form. However, interferometers need lots of auxiliaries for aspherics, such as compensators.

(2) JR-1800 is competent for any kind of surface quality, including specular and nonspecular surfaces. Interferometers cannot test rough surfaces due to mass scattering of laser.

(3) JR-1800 supplies the sagittal heights of the sampling points, which can be used to fit aspheric parameters such as the vertex curvature and conic coefficient. This cannot be obtained directly by interferometers.

(4) As a mechanical instrument, the measurement accuracy of JR-1800 is relatively lower than that of interferometers. This system is expected to achieve an accuracy of ∼1 μm and guide lapping or initial polishing processes.

(5) The intrinsic measuring time of JR-1800 is much longer than that of interferometers. The

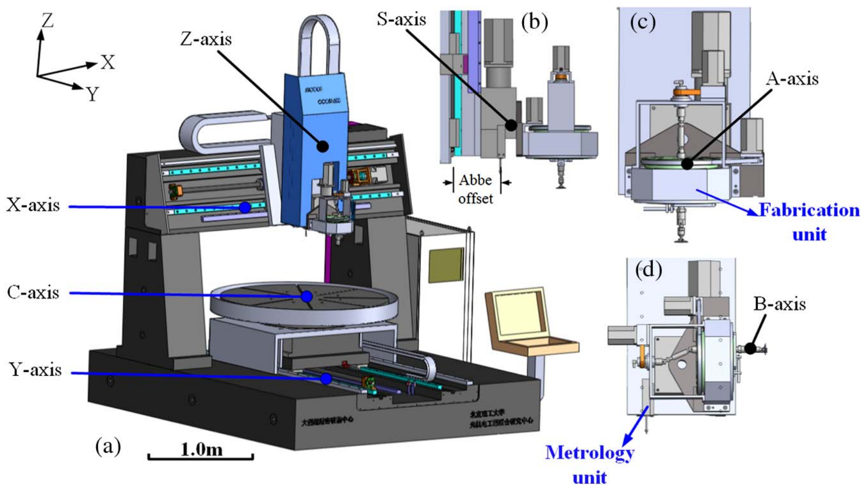

Fig. 2. Schematic illustration of JR-1800: (a) overall view; (b) lateral view of the metrology and fabrication units; (c) fabrication status; and (d) metrology status.

maximal speed is ~2000 points per hour and is usually at 1000–1200. However, as the measurement is *in situ*, it saves time for carrying and remounting the workpieces, so, the equivalent measuring time is nearly in of the same order of magnitude with that of interferometers.

3. Calibrations and Alignments of JR-1800

A. Calibrations of Mechanical Errors

For JR-1800, the mechanical errors influencing measurement results involve linearity error of guide rails, positioning error of linear or rotating axes, etc. Mechanical errors are inherent errors, which remain invariant over quite a long time. Therefore, they can be calibrated precisely. Here, the linearity and positioning errors of $XYZC$ axis are measured with a Renishaw XL-80 interferometer as listed in Table 1. The positioning error is less than 6.0 μm for XY axis and 9.2 s for C axis, while repeat positioning error is ~3.3 μm for XY axis and 4.3 s for C axis. While moving 1600 mm, the linearity of X axis is 1.75 μm, which has a 100% print-through effect on the measurement results. This high mechanical precision is a basic guarantee for profile measurement on JR-1800.

There are also other mechanical errors that degrade the measurement accuracy of JR-1800, such as the radial and axial run-out of C axis; the parallelism of X axis and the turntable; the perpendicularity of XY axis, XZ axis, and YZ axis, and so on. It is hard to correlate them with the measuring results. In this work, a calibration method is used to measure the synthetic systemic error caused by the mechanical errors of JR-1800.

The calibration process measures a 440 mm × 440 mm standard window with JR-1800. The window has a surface form of PV = 0.23 μm, RMS = 0.029 μm, measured by a 24 in. (~610 *mm*) Zygo laser interferometer. The calibration results on JR-1800 with XC mode and XY mode (removing the surface form measured by Zygo) are presented in Fig. 3. For XC mode [Fig. 3(a)], the error map generally shows rotational symmetry, with PV = 2.32 μm, RMS = 0.38 μm. The error map for XY mode [Fig. 3(b)] has PV = 3.0 μm, RMS = 0.53 μm. The two error maps are quite different because they represent different combinations of the mechanical errors of JR-1800. They serve as the system error of JR-1800 and should be first removed from a measuring result.

By the way, the two calibrations just obtain the systemic error at the center of the turntable (a 440 mm × 440 mm square). A full-aperture calibration for the Φ1800 mm turntable is necessary for measuring meter-scale workpieces. Correlative works are now designed and a stitching method is preliminarily confirmed. This method measures the window multiple times with JR-1800 while realigning the window to cover the full aperture of the turntable, and correlating results will be reported in a later work.

Table 1. Mechanical Errors of ***XYZC*** Axis

Axis	Positioning Accuracy	Repeat Positioning Accuracy	Slider Linearity	Measured Range
X	5.9 μm	3.3 μm	1.75 μm	1600 mm
Y	5.6 μm	3.2 μm	4.30 μm	2000 mm
Z	2.2 μm	1.3 μm	1.66 μm	600 mm
C	9.2 s	4.3 s	—	360°

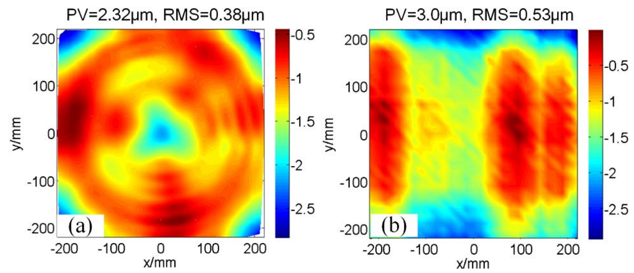

Fig. 3. Calibration results of the systemic error of JR-1800 with (a) XC mode and (b) XY mode.

B. Misalignments of the Length Gauge and Workpiece

As shown in Fig. 4(a), there are three important coordinates: (1) the measurement coordinate (O_m-$X_mY_mZ_m$) located at the center of the turntable; (2) the workpiece coordinate (O_w-$X_wY_wZ_w$) built in the vertex of the workpiece; and (3) the metrology tool coordinate (O_t-$X_tY_tZ_t$) originating at the ball tip mounted on the plunger of the length gauge. Theoretically, these three coordinates should be aligned together in XY direction as shown in Fig. 4(b). The alignments for JR-1800 that are carried out carefully to enhance the measurement accuracy are described as follows.

1. *Alignment of Length Gauge*

To illustrate the influence of misalignments on measurement results, here we assume six Φ1000 mm parabolic segments with different F numbers (F#) that are measured by JR-1800. The first series investigates the measurement error caused by increasing offset in X direction. Assuming $F\# = 2$, the surface function can be expressed as Eq. (7). If the offset increases from 10 to 90 μm, the resulting error can be expressed by Eq. (8) and is plotted in Fig. 5(a). The curves show a linear, directly proportional relation to

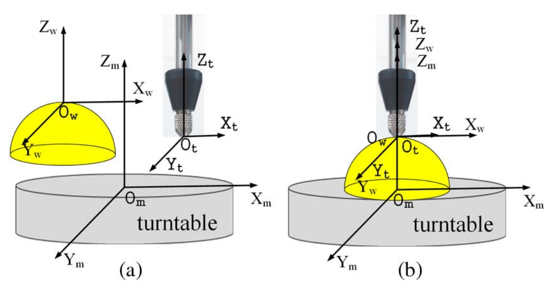

Fig. 4. Coordinates of JR-1800 (a) with offset in XY direction and (b) aligned together precisely in XY direction.

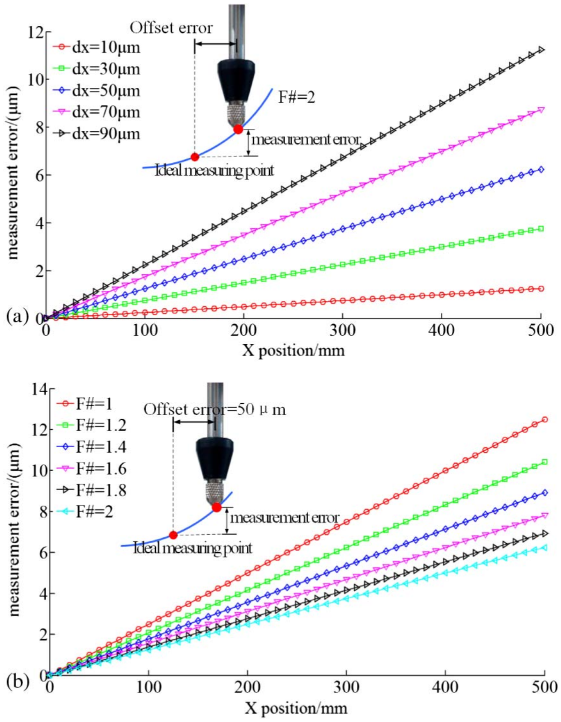

Fig. 5. Emulational measurement errors caused by tool misalignment (a) with different offsets and (b) with different *F*#.

X position (i.e., radial distance). And the error would be enlarged when the offset error increases, which reaches 11.30 μm for 90 μm offset at the edge. In addition, an offset error of 10 μm would induce a measurement error of more than 1 μm at the edge region.

The second set investigates the influence of tool offset on measurement error for segments with different $F\#$. As shown in Fig. 5(b), when $F\#$ varies from $F\# = 2$ to $F\# = 1$, the measurement errors are enlarged one by one, which indicates that the offset has a larger influence on steeper (i.e., higher slope) surfaces.

$$X^2 = 2RZ, \tag{7}$$

$$dz = \frac{(X+dx)^2}{2R} - \frac{X^2}{2R} = \frac{2Xdx + dx^2}{2R} \approx \frac{Xdx}{R}. \tag{8}$$

According to the above analysis, the alignment errors should be calibrated carefully after remounting the tool because they would directly influence the measurement results. Over a quite long usage time, calibration can ensure high measurement accuracy, except for remounting the metrology tool. The tilt error can be calibrated easily with a dial gauge contacting the extending plunger, ensuring it has variation less than 1 μm when moving Z axis up and down for ~50 mm. The tool offset can also be aligned by rotating the dial gauge along the plunger (the gauge tip leaning against the side surface of the plunger). However, this method is invalid if the plunger is not a cylinder or the sensor is a noncontact tool such as a laser triangle or a confocal displacement sensor.

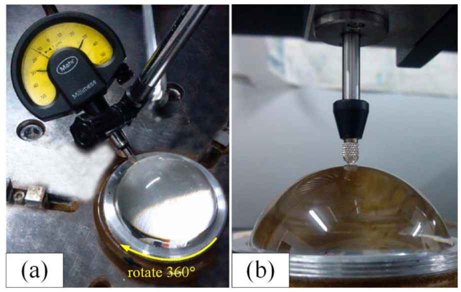

Fig. 6. Calibration model for misalignments of the length gauge in XY position.

In this work, we present a quantitative method to reduce the offset of MT60, which utilizes a dial gauge (0.001 mm resolution) and a standard sphere (optical surface of 0.2 μm level, radius 30 mm). The calibration procedure is described in Fig. 6. First, the standard sphere is aligned at the center of the turntable with a dial gauge. As shown in Fig. 6(a), the tip of the dial gauge contacting the standard sphere is aligned; then the turntable is rotated by 360° continuously, while realigning the XY position of the standard sphere to ensure the variation of the dial gauge is less than 1 μm during the rotation process. The second step measures a profile along X direction with MT60 as shown in Fig. 6(b) and gets a series of discrete data. Theoretically, the tool measures the profile of an exact radius, but due to the alignment errors, the factual measuring data deviate from the radius, which can be predicted by Eq. (9) where R_0 denotes the radius of the standard sphere. Subtract the ideal data from the measurement data [Eq. (10)], the measurement square error can be expressed as Eq. (11), from which we can see that the square error has a reverse linear proportional relation with the offset along X axis, dx. Then, dx can be fitted by the least-square method. The third step measures the alignment error in Y direction like the second step. Attention is paid so that the data measured would be preprocessed to remove the error resulting from the radius of the tool tip (a Φ3.2 mm sphere). According to our measurement, alignment errors have remained in the tool tip after pre-centering are 13.6 μm and 41.2 μm in X and Y directions, as shown by Eq. (12); these were calibrated by redefining the centering XY position. Some random errors, such as mounting error and the surface error of the standard sphere, tool measurement error, etc., would influence the accuracy of this method; but if this alignment is repeated 2 or 3 times, the offset error can be restricted to within ±5 μm:

$$Z'^2 = R_0^2 - ((X+dx)^2 + dy^2) \approx R_0^2 - (X^2 + 2Xdx), \tag{9}$$

$$Z^2 = R_0^2 - X^2, \tag{10}$$

$$\delta = Z'^2 - Z^2 = -2Xdx, \tag{11}$$

$$dx = 13.6\ \mu\text{m}, \qquad dy = 41.2\ \mu\text{m}. \tag{12}$$

2. Alignments of Workpieces

After a workpiece is mounted on the turntable, its position should be adjusted to align to the center of the turntable. If the workpiece has a high-quality cylinder side surface, it can be centered well by inspecting the variation of a dial gauge with the tip leaning against the side face of the workpiece while rotating the turntable by 360°. However, with respect to an irregular workpiece, such as ellipses or hexagons, this method would be invalid. Here, a surface-measured method is presented. If an aspherical mirror has offset error (dx, dy), the measured error of a circle (radial distance ρ) can be expressed as Eq. (13), which indicates that the error would be a trigonometric function of the rotation angle θ. Assuming $dx = 0.2$ mm and $dy = 0.3$ mm, if ρ increases from 10 to 50 mm, the ideal measurement data can be obtained from Eq. (13) and are plotted as shown in Fig. 7.

Equation (14) represents the evaluating function for the least-square fitting method, which should satisfy Eq. (15) to ensure a least-square solution. Then, Eq. (15) is derived as Eq. (16). By a matrix division operation, the offset errors of the workpiece can be obtained easily. As our test on a Φ320 mm circular workpiece, repeating this aligning process for three times, it can be centered with about ±3 μm deviation (measured by a dial gauge sliding around the side surface).

$$dz = -\frac{C\rho\,\cos(\theta)}{\sqrt{1-(K+1)C^2\rho^2}}dx + \frac{C\rho\,\sin(\theta)}{\sqrt{1-(K+1)C^2\rho^2}}dy, \tag{13}$$

$$S(dx, dy) = \sum_{i=1}^{n}[Z_i - dz_i]^2 = \sum_{i=1}^{n}[Z_i - (U_i dx + V_i dy)]^2, \tag{14}$$

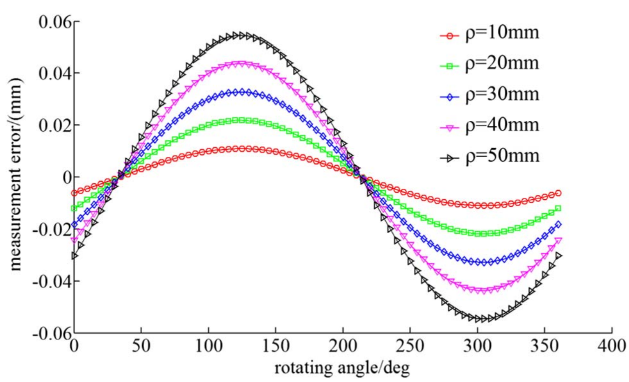

Fig. 7. Measurement error if the workpiece has offset error.

$$\frac{\partial S}{\partial dx} = \frac{\partial S}{\partial dy} = 0, \tag{15}$$

$$\begin{vmatrix} \sum U_i^2 & \sum U_i V_i \\ \sum U_i V_i & \sum V_i^2 \end{vmatrix} \begin{vmatrix} dx \\ dy \end{vmatrix} = \begin{vmatrix} \sum Z_i U_i \\ \sum Z_i V_i \end{vmatrix}, \tag{16}$$

$$U_i = \frac{-C\rho_i\,\cos(\theta_i)}{\sqrt{1-(K+1)C^2\rho_i^2}} V_i = \frac{C\rho_i\,\sin(\theta_i)}{\sqrt{1-(K+1)C^2\rho_i^2}}. \tag{17}$$

C. Output Stability of MT60

The output stability of the length gauge also has a significant influence on the measurement results. When the plunger strikes an object, the data read by its controller (e.g., IK220) are varying back and forth within a magnitude of ~0.02–0.05 μm; so reading the data only once for every strike may incur a measurement error. This work studies the influence of reading times on output stability by striking the same point of an object 100 times, with different reading times for every strike.

Figure 8 gives the PV and RMS of output the output stability of MT60 with different reading times ($n = 1$ to $n = 200$) for 200 strikes on a the same position; it can be seen that two the two curves reach an asymptote when $n \geq 20$ and the PV value can be controlled restricted within to within 0.08 μm. The reading times is reasonable from $n = 20$ to $n = 50$. By the way, the controller can read the position of the plunger ~10,088 times per second.

D. Influence of Temperature on Measurement Results

Temperature variation also induces the deformation of JR-1800, which reduces the measurement accuracy. Here, the FEA method is adopted to simulate the deformation of JR-1800 due to temperature variation. The machine was meshed with a size of 50 mm, producing 731,444 elements. The material parameters are listed in Table 2. Figure 9 presents the deformation of the machine when the temperature increases 1°C (reference at 20°C). The maximal deformation is ~23 μm. The measurement results are prone to be influenced by deformations of the mounting positions of the length gauge (point A in Fig. 9) and the supporting workpiece (point B in Fig. 9). The deformation difference at points A and B is

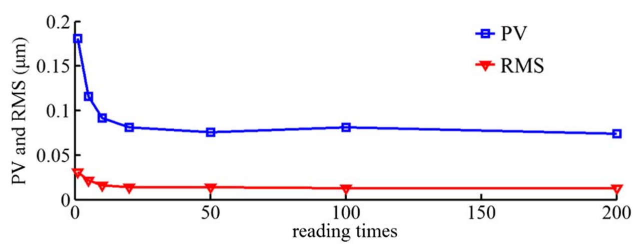

Fig. 8. Output stability with increasing reading times.

Table 2. Parameters of Materials

Parameter	Marble	45# Steel	Cast Iron
Density (kg/m^3)	3070	7750	7850
Young's modulus (Pa)	6.0E + 10	1.93E + 11	1.5E + 11
Poisson ratio	0.25	0.31	0.27
Shear modulus (Pa)	2.4E + 10	7.69E + 10	4.77E + 10
Bulk modulus (Pa)	4.0E + 10	1.67E + 11	1.46E + 11
Coefficient of thermal expansion (/K)	4.6E − 6	12E − 6	10.2E − 6
Thermal conductivity (W/m/K)	3.0	60.5	51.5

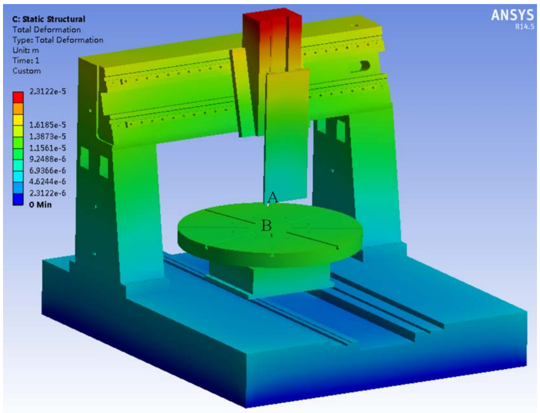

Fig. 9. Deformation diagram of the proposed system when temperature increases by 1°C.

0.91 μm/°C. Indeed, the temperature of JR-1800 is maintained at 20 ± 0.2°C; then the maximal error induced by temperature variation is about ±0.182 μm.

Deformation of MT60 due to temperature variation should also be considered. According to the specification of MT60, the temperature dependence is 0.16 μm/°C. Then, the error induced at ±0.2°C is 0.032 μm. The influence of temperature on the deformation of the workpieces depends on the dimension and material of the workpieces, and should be analyzed in particular.

E. Vibration Mode and Natural Frequency of JR-1800

Modal analysis can confirm the fundamental vibration mode shapes and the corresponding frequencies. Here, the vibration modes of JR-1800 are analyzed and its natural frequencies are confirmed by FEA. The first six order modal analysis and relative frequencies are given in Fig. 10, inducing different pitches, rolling, torsions, and bending to XZ axis. Thereinto, all of these six vibrations would induce a large deformation to the mounting position of the length gauge, which is ~113 μm in maximal. Therefore, these validation shapes should be avoided in the measuring process. It should be noted that the first natural frequency is 56.289 Hz, which is far more than the operating frequency of the seven servo motors. Thus, these fundamental vibration modes can be avoided for JR-1800.

4. Error Compensation

A. Tool Radius Compensation

As in the model illustrated in Fig. 11, as the tool tip has a sphere with radius $R_t = 1.6$ mm, the factual contact point Q on the curved surface is not the point to be measured (point P), and the length gauge gives

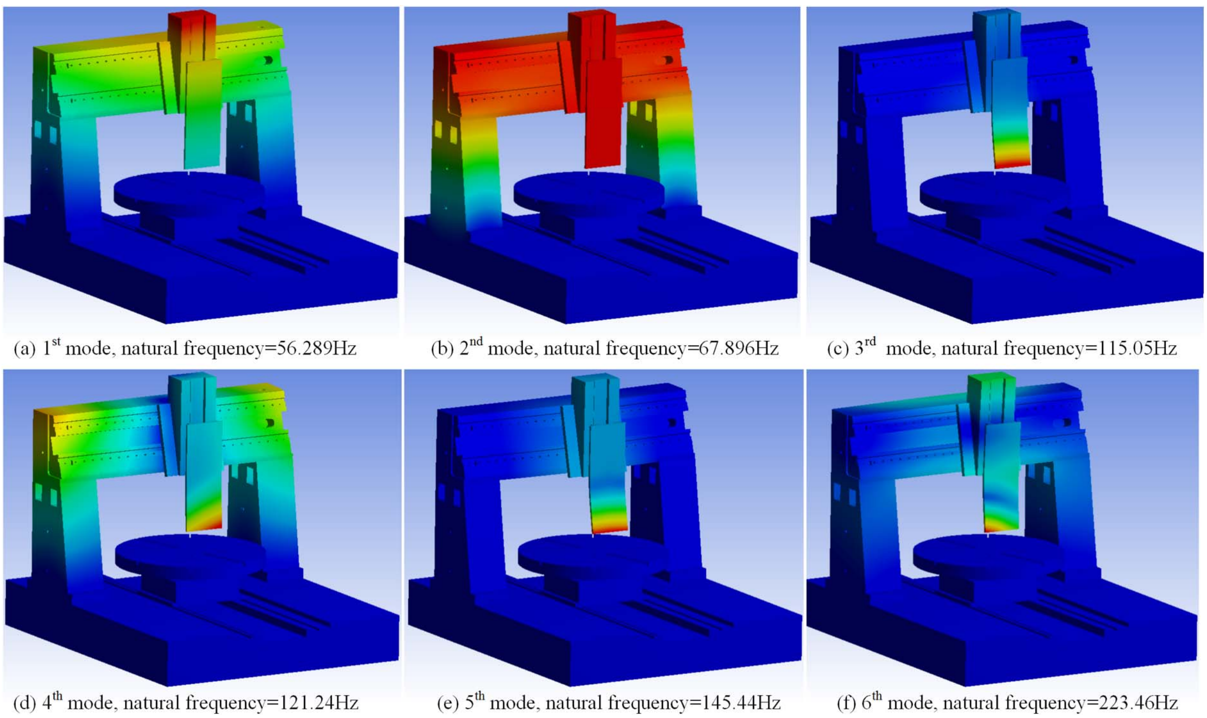

Fig. 10. First six mode vibration shapes and the corresponding natural frequencies.

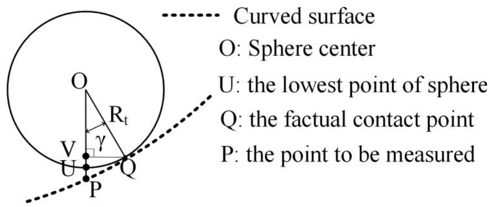

Fig. 11. Sketch map of tool radius compensation.

the sagittal height of point U (the lowest point on the sphere), which consequently induces a nonlinear error in the measurement results. A common method to eliminate this error is adding or subtracting the theoretical sagittal deviations of points U and P as shown in Eq. (18), where X_P and Y_P are given by the measurement path, Z_Q and Z_P can be given by Eq. (1), and γ is the angle between the normal vector of Q and Z axis. Moreover, the tip sphere is made of special hard-wearing steel and can be replaced by a new one. Thus, tool wear is not considered.

$$\begin{aligned} Z_{UP} &= Z_{VP} - Z_{VU} = Z_Q - Z_P - Z_{VU} \\ &= Z(\sqrt{(X_P^2 + Y_P^2)} + R_t \sin(\gamma), 0) \\ &\quad - Z(\sqrt{(X_P^2 + Y_P^2)}, 0) - R_t(1 - \cos(\gamma)). \end{aligned} \tag{18}$$

B. Tilt and Offset Compensation

The calibrations and alignments mentioned above can suppress the degeneration of measurement accuracy, but cannot eliminate misalignment errors completely. A compensation model is then presented to eliminate residual misalignments, which takes the tilt and offset errors into account simultaneously.

As shown in Fig. 12, in O-XYZ, O is the center of the turntable. Theoretically, O'-$x'Y'Z'$ (i.e., the workpiece coordinate) should be coincident with O-XYZ. Due to the existence of a tilt error (α, β) and an offset error (dx, dy), the practical surface acts as the blue curve as in Fig. 12. Take a two-order aspherical surface as an example; if we measure point $A(X_A, Y_A, Z_A)$ on the ideal surface, actually we get the sagittal height of $B(X_B, Y_B, Z_B)$ on the practical

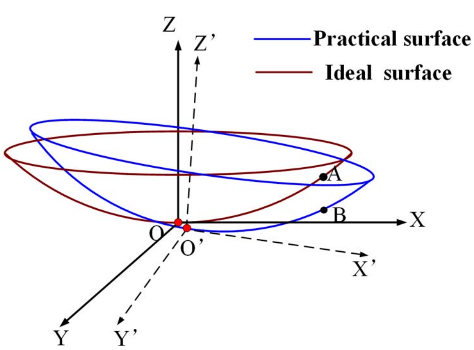

Fig. 12. Schematic illustration of the error separation model.

surface. As the tool stretches out, its plunger is oriented perpendicular to the XOY plane; then we have Eq. (19):

$$X_A = X_B, \qquad Y_A = Y_B. \tag{19}$$

Therefore, the measurement error dz is the height difference between A and B, as shown in Eq. (20). Z_A could be obtained from Eq. (1). To get dz, we need to know Z_B. In O'-$x'Y'Z'$, the coordinate of B, (X'_B, Y'_B, Z'_B) can be obtained from Eq. (21):

$$dz = Z_B - Z_A, \tag{20}$$

$$\begin{vmatrix} X'_B \\ Y'_B \\ Z'_B \\ 1 \end{vmatrix} = \left(\begin{bmatrix} \cos(\beta) & \sin(\beta)\sin(\alpha) & \sin(\beta)\cos(\alpha) & d_x \\ 0 & \cos(\alpha) & -\sin(\alpha) & d_y \\ -\sin(\beta) & \cos(\beta)\sin(\alpha) & \cos(\beta)\cos(\alpha) & 0 \\ 0 & 0 & 0 & 1 \end{bmatrix} \right)^{-1} \times \begin{vmatrix} X_B \\ Y_B \\ Z_B \\ 1 \end{vmatrix}. \tag{21}$$

In O'-$x'Y'Z'$, (X'_B, Y'_B, Z'_B) satisfies Eq. (1). Combining Eqs. (21) and (1), and removing high-order small data, we get Eq. (22):

$$\begin{aligned} &(K+1)Z_B^2 + 2(KX_B \sin(\beta) - KY_B \sin(\alpha) - R)Z_B \\ &+ X_B^2 + Y_B^2 - 2X_B dx - 2Y_B dy - 2RX_B \sin(\beta) \\ &+ 2RY_B \sin(\alpha) = 0. \end{aligned} \tag{22}$$

Equation (22) is the equation of the practical surface in O-XYZ. Assign practical surface equation $z_1 = f_1(x, y)$; Eq. (22) could be simplified as Eq. (23) and solved as Eq. (24). So dz is derived as in Eq. (25), which is separated as the summation of dx, dy, $\sin(\alpha)$, and $\sin(\beta)$:

$$az_1^2 + bz_1 + c = 0, \tag{23}$$

$$\text{where} \begin{cases} a = 1 + K \\ b = 2Kx\sin(\beta) - 2Ky\sin(\alpha) - 2R \\ c = x^2 + y^2 - 2xdx - 2ydy - 2Rx\sin(\beta) + 2Ry\sin(\alpha) \end{cases},$$

$$z_1 = \begin{cases} \frac{-b+\sqrt{b^2-4ac}}{2a} & (K \neq -1) \\ -c/b & (K = -1) \end{cases}, \tag{24}$$

$$\begin{cases} dz = \frac{1}{K+1}\left[\left(K + \frac{1}{\sqrt{1-(K+1)C^2(x^2+y^2)}}\right)y\ \sin(\alpha) - \left(K + \frac{1}{\sqrt{1-(K+1)C^2(x^2+y^2)}}\right)x\ \sin(\beta)\right] - \frac{xdx+ydy}{\sqrt{1-(K+1)C^2(x^2+y^2)}} & (K \neq -1) \\ dz = \left[-x - \frac{(x^2+y^2)}{2R^2}x\right]\sin(\beta) + \left[y + \frac{(x^2+y^2)}{2R^2}y\right] \sin(\alpha) - Cxdx - Cydy & (K = -1) \end{cases}. \quad (25)$$

These errors can be fitted by the least-square algorithm. As an example of $K \neq -1$, assign $S = dx$, $T = dy$, $U = \sin(\alpha)$, $V = \sin(\beta)$, and

$$\begin{cases} s_i = \frac{Cx_i}{\sqrt{1-(K+1)C^2(x_i^2+y_i^2)}} \\ t_i = \frac{Cy_i}{\sqrt{1-(K+1)C^2(x_i^2+y_i^2)}} \\ u_i = \frac{1}{K+1}\left(K + \frac{1}{\sqrt{1-(K+1)C^2(x_i^2+y_i^2)}}\right)y_i \\ v_i = -\frac{1}{K+1}\left(K + \frac{1}{\sqrt{1-(K+1)C^2(x_i^2+y_i^2)}}\right)x_i \end{cases}. \quad (26)$$

Then the ideal measurement error can be expressed as

$$dz = s_i * S + t_i * T + u_i * U + v_i * V. \quad (27)$$

Define $W(S,T,U,V)$ as in Eq. (28), where dz' denotes the actual measurement error:

$$W(S,T,U,V) = \sum_{i=1}^{n}[dz' - dz]^2 = \sum_{i=1}^{n}[dz' - (s_iS + t_iT + u_iU + v_iV)]^2. \quad (28)$$

Based on the least-square method, Eq. (28) should satisfy Eq. (29), which can be simplified as Eq. (30). Solving it by the numerical computation method, S, T, U, and V can be obtained; then we can get dz and the final surface form:

$$\frac{\partial W}{\partial S} = \frac{\partial W}{\partial T} = \frac{\partial W}{\partial U} = \frac{\partial W}{\partial V} = 0, \quad (29)$$

$$\begin{vmatrix} \sum s_i^2 & \sum s_it_i & \sum s_iu_i & \sum s_iv_i \\ \sum t_is_i & \sum t_i^2 & \sum t_iu_i & \sum t_iv_i \\ \sum u_is_i & \sum u_it_i & \sum u_i^2 & \sum u_iv_i \\ \sum v_is_i & \sum v_it_i & \sum v_iu_i & \sum v_i^2 \end{vmatrix} \begin{vmatrix} S \\ T \\ U \\ V \end{vmatrix} = \begin{vmatrix} \sum dz's_i \\ \sum dz't_i \\ \sum dz'u_i \\ \sum dz'v_i \end{vmatrix}. \quad (30)$$

5. Experiments for Feasibility Validation of JR-1800

A. Validation Experiments for Repeatability

A Φ400 mm optical plane is measured three times by JR-1800 for repeatability. The process employs a concentric circle path with a space interval of 8 mm, with 2030 points in total, and takes about 85 min; the ambient temperature is 20.0 ± 0.1°C. The surface forms after compensation are given in Fig. 13, which show high coincidence with each other in surface form distribution. The RMS deviation of the three measurements is less than $1/30\lambda$, which validates that JR-1800 has high repeatability (RMS $< 1/30\lambda$).

B. Validation Experiments for Measurement Accuracy

To validate the measurement accuracy of JR-1800, the above workpiece is measured with a 24 in. Zygo interferometer as shown in Fig. 14(a), with PV $= 1.249\lambda$, RMS $= 0.231\lambda$. The RMS deviation of JR-1800 from Zygo is 0.013λ. Comparing the surface forms of the two instruments, we can find that JR-1800 can provide reliable data with a highly

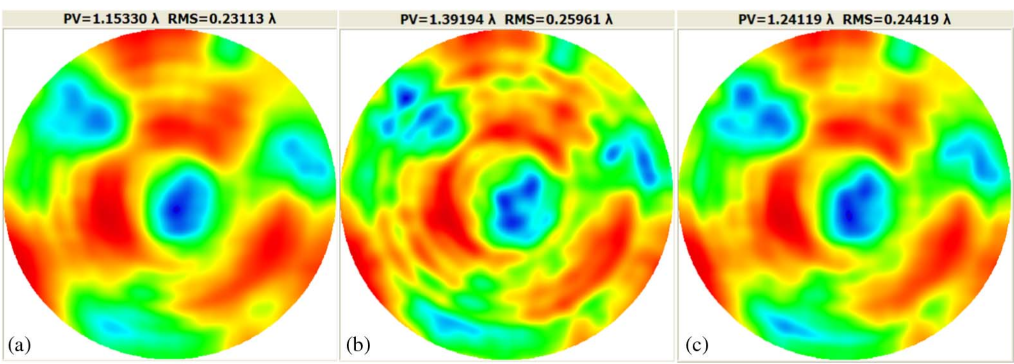

Fig. 13. Comparing the results of a plane measured with JR-1800: (a) first, PV $= 1.15\lambda$, RMS $= 0.231\lambda$; (b) second, PV $= 1.39\lambda$, RMS $= 0.259\lambda$; and (c) third, PV $= 1.24\lambda$, RMS $= 0.244\lambda$.

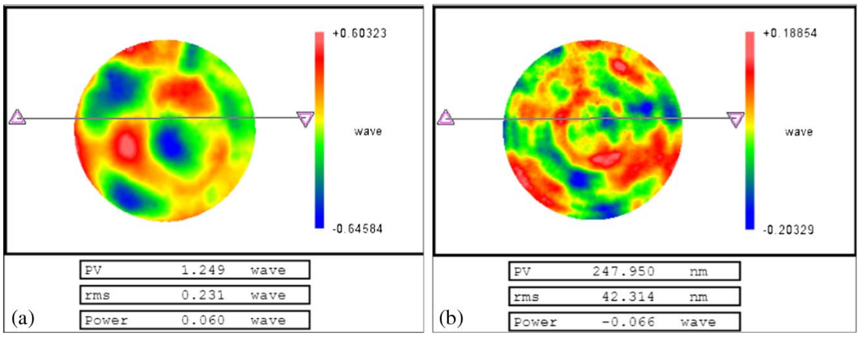

Fig. 14. (a) Result of Zygo GPI laser interferometer: PV = 1.25λ, RMS = 0.231λ. (b) Direct subtraction of the measurement results of JR-1800 and Zygo interferometer, PV = 248 nm, RMS = 42 nm.

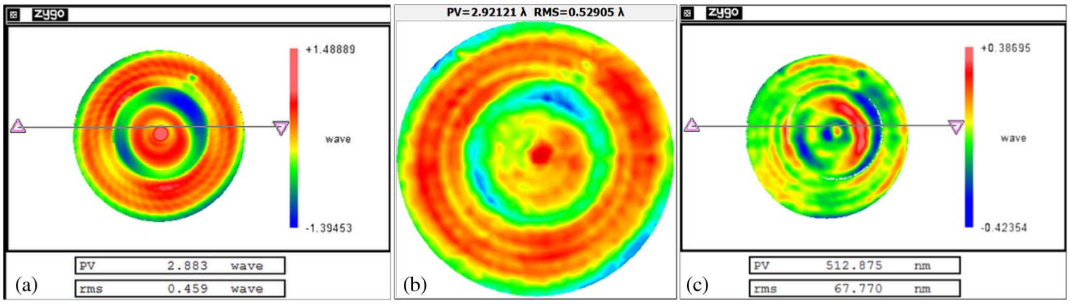

Fig. 15. (a) Interferometric result with Zygo PGI laser interferometer: PV = 2.88λ, RMS = 0.459λ. (b) Result measured with JR-1800: PV = 2.92λ, RMS = 0.529λ. (c) Direct subtraction of the measurement results of JR-1800 and Zygo interferometer: PV = 512 nm, RMS = 67.8 nm.

coincident surface form distribution to interferometers. In addition, utilizing the averaged data of JR-1800 to subtract the interferometric result, the relative measurement error presented in Fig. 14(b) indicates that PV is 0.247 μm and RMS is 0.042 μm, which validates that JR-1800 can be used for guiding the lapping and initial polishing of optical mirrors.

C. Validation Experiments for Aspherical Mirrors

Figure 15(a) presents the measurement results of a Φ320 mm ($R = 4000$) paraboloid by Zygo laser interferometer (with an optical null compensator). It shows 2.88λ PV and 0.459λ RMS (with tilt and defocus removed). A concentric circle path with 2900 points (15 mm interval) is used in the measurement process of JR-1800, which costs 143 min. The result shown in Fig. 15(b) indicates PV = 2.92λ, RMS = 0.529λ. It can be seen that the surface form distributions measured by two systems have high resemblance. The RMS deviation from the interferometric result is 0.07λ. Direct subtraction of the two results is shown in Fig. 15(c), which indicates that PV is 0.512 μm and RMS is 0.067 μm. The results given by JR-1800 can be used for guiding the lapping or initial polishing of large aspheric mirrors.

6. Conclusions

In this work, the profile measurement of aspherics by an on-machine 3D profile measurement system (JR-1800) is investigated in detail. The measurement errors induced by mechanical errors, misalignments of the length gauge and workpieces, the output stability of the length gauge, temperature variation, and natural vibrations are analyzed. The synthetic systemic error is calibrated by measuring a standard window. Two quantitative methods are presented for aligning the length gauge, turntable, and workpiece together. The influences of temperature variation and fundamental vibrations on measurement results are simulated by the FEA method, which confirms that the temperature dependence is 0.91 μm/°C, and the first natural vibration frequency is much higher than the operating frequencies of the machine. In particular, tool radius and misalignment compensation models are built. The system is validated to be effective by two experiments, in which RMS repeatability reached 1/30λ, and direct subtraction of the measurement results with JR-1800 and Zygo laser interferometer revealed that the RMS deviation is less than 0.07 μm for both workpieces.

This work was supported by the National Natural Science Foundation of China (Grant Nos. 61308075 and 61222506) and the Specialized Research Fund for the Doctoral Program of Higher Education (Grant No. 20131101110026).

References

1. P. Comley, P. Morantz, P. Shore, and X. Tonnellier, "Grinding metre scale mirror segments for the E-ELT ground based telescope," CIRP Ann. **60**, 379–382 (2011).
2. J. C. Lambropoulos, S. Xu, and T. Fang, "Loose abrasive lapping hardness of optical glasses and its interpretation," Appl. Opt. **36**, 1501–1516 (1997).

3. Z. C. Dong, H. B. Cheng, and H. Y. Tam, “Investigation on removal features of multidistribution fixed abrasive diamond pellets used in the polishing of SiC mirrors,” Appl. Opt. **51**, 8373–8382 (2012).
4. H. B. Cheng, Z. J. Feng, K. Cheng, and Y. W. Wang, “Design of a six-axis high precision machine tool and its application in machining aspherical optical mirrors,” Int. J. Mach. Tools Manuf. **45**, 1085–1094 (2005).
5. H. B. Cheng, Y. Yam, and Y. T. Wang, “Experimentation on MR fluid using a 2-axis wheel tool,” J. Mater. Process. Technol. **209**, 5254–5261 (2009).
6. J. Burke, K. Wang, and A. Bramble, “Null test of an off-axis parabolic mirror. I. Configuration with spherical reference wave and flat return surface,” Opt. Express **17**, 3196–3210 (2009).
7. Y. F. Wen, H. B. Cheng, and H. Y. Tam, “Modified stitching algorithm for annular subaperture stitching interferometry for aspheric surfaces,” Appl. Opt. **52**, 5686–5694 (2013).
8. P. Zhou and J. H. Burge, “Optimal design of computer-generated holograms to minimize sensitivity to fabrication,” Opt. Express **15**, 15410–15417 (2007).
9. E. P. Goodwin and J. C. Wyant, *Field Guide to Interferometric Optical Testing* (SPIE, 2006).
10. R. S. Breidenthal, “Measurement of large optical surfaces for fabrication using a non-optical technique,” Proc. SPIE **1618**, 97–103 (1991).
11. C. Gray, I. Baker, and G. Davies, “Fast manufacturing of E-ELT mirror segments using CNC polishing,” Proc. SPIE **8838**, 88380k (2013).
12. P. Su, C. J. Oh, R. E. Parks, and J. H. Burge, “Swing arm optical CMM for aspherics,” Proc. SPIE **7426**, 74260J (2009).
13. P. Su, Y. H. Wang, C. J. Oh, R. E. Parks, and J. H. Burge, “Swing arm optical CMM: self-calibration with dual probe shear test,” Proc. SPIE **8126**, 81260 (2011).
14. H. W. Jing, C. King, and D. Walker, “Simulation and validation of a prototype swing arm profilometer for measuring extremely large telescope mirror-segments,” Opt. Express **18**, 2036–2048 (2010).
15. H. W. Jing, C. King, and D. Walker, “Measurement of influence function using swing arm profilometer and laser tracker,” Opt. Express **18**, 5271–5281 (2010).
16. F. J. Chen, S. H. Yin, H. Huang, H. Ohmori, Y. Wang, Y. F. Fan, and Y. J. Zhu, “Profile error compensation in ultra-precision grinding of aspheric surfaces with on-machine measurement,” Int. J. Mach. Tools Manuf. **50**, 480–486 (2010).
17. Z. C. Dong, H. B. Cheng, and H. Y. Tam, “Modified subaperture tool influence functions of a flat pitch polisher with reverse-calculated material removal rate,” Appl. Opt. **53**, 2455–2464 (2014).